A NEW METHOD FOR QUANTITTATIVE REFLECTION IMAGING

Jian-Yu Lu and Yu Wei

Department of Biomedical Engineering
Nanjing Institute of Technology
Nanjing, China

INTRODUCTION

B-scanner is one of the most successful medical ultrasonic diagnostic equipment developed in 1970s. It can provide the outline images of the internal structures of the cross-sections of the biological soft-tissues and is useful in diagnosing the diseases of the shape abnormalities of the tissues, such as, tumors in livers, kidneys, etc.. Although great efforts have been done to further improve the quality of B-scan images[1-9], the ordinary B-scanner can not provide the quantitative images of the distributions of the acoustical parameters of the biological soft-tissues. In this paper, a new quantitative reflection imaging method (short for QRI method) is developed, which is directly based on the acoustical transmitting/receiving geometry of the ordinary B-scanner and can provide a quantitative image of the sound speed distribution of the biological soft-tissues and will be useful in tissue characterization.

The imaging procedure of the QRI method is as follows. First, the high-frequency component of one-dimensional object function (i.e., the object function on the line through which a focused pulse acoustical wave is propagated) is obtained from the rf (radio frequency) echo signals returned from the object. Then, the low-frequency component of the one-dimensional object function is determined from the high-frequency component using the GP (Gerchberg-Papoulis) frequency extrapolation technique[10] and using the a priori knowledges that the outlines of the internal structures of the object and the phases of the rf echo signals returned from these outlines are known. From the complete frequency spectrum, the one-dimensional object function can be reconstructed. By scanning the focused pulse acoustical wave in the cross-section of the object to be imaged, the two-dimensional object function in that cross-section can be reconstructed.

In addition, an experimental system which connects the B-scanner to computer is developed for the datum acquisition of the rf echo signals, and images of practical objects are reconstructed using the data obtained by this experimental system. The results show that the images reconstructed by the QRI method are more helpful in understanding the internal structures of the testing objects than the ordinary B-scan images, and to a certain extent, the images are quantitative.

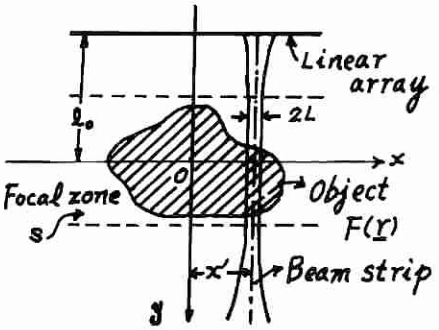

Fig.1 Datum acquisition geometry of the QRI method

BASIC PRINCIPLES

Theoretical Preliminaries

Fig.1 is the datum acquisition geometry of the QRI method. The x-y coordinates are fixed in the space; $F(\underline{r})$ represents the two-dimensional object function (objects are located in an echoless water-tanker and in the focal zone of the linear array probe); L is the half-width of the focused ultrasonic beam; x' indicates the distance of the center of the beam to the y-axis and l_0 is the distance between the surface of the linear array probe and the x-axis. The linear array probe used here is consist of many small transducer elements and can be scanned electrically, it is used both as transmitter and receiver. The focal zone of the linear array probe is defined as the region where the ultrasonic beams produced are focused so narrow and even that they can be approximately looked as a plane wave within the width of each beam strip.

In this paper, the incident wave used is a pulse acoustical wave. For the pulse acoustical wave can be decomposed into monochromatic wave with different frequencies, in the following, we will first consider the case of the monochromatic wave. Suppose that the acoustical waves interacting with the biological soft-tissues are governed by the following Helmholtz equation[11]

$$\nabla^2 U(\underline{r})+k_0^2 U(\underline{r}) = -F(\underline{r})U(\underline{r}) \tag{1}$$

where $U(\underline{r})$ represents the total sound pressure field; $k_0 = \omega/c_0$ is the wavenumber of the homogeneous medium which surrounds the object (ω is the angular frequency of the incident wave and c_0 is the sound speed of the surrounding homogeneous medium). The object function $F(\underline{r})$ is given by

$$F(\underline{r}) = \begin{cases} k_0^2[n^2(\underline{r})-1]; & \text{if } \underline{r} \text{ is in the object} \\ 0 \qquad\qquad ; & \text{otherwise} \end{cases} \tag{2}$$

where $n(\underline{r})$ represents the distribution of the refractive index of the object and is related to the sound speed distribution by $n(\underline{r}) = c_0/c(\underline{r})$. Considering the first-order Born approximation (i.e., weak scattering assumption is assumed), one obtains the following integral solution of Eq.(1)[12]

$$U_s(\underline{r}) = \int_s F(\underline{r}_0)U_i(\underline{r}_0)g(\underline{r}|\underline{r}_0)d\underline{r}_0 \tag{3}$$

where $U_s(\underline{r})$ and $U_i(\underline{r})$ represent scattered field and incident field respectively, (the total field $U(\underline{r})$ is the sum of $U_i(\underline{r})$ and $U_s(\underline{r})$); the

integral area s is the focal zone of the linear array probe, as shown in Fig.1; $g(\underline{r}|\underline{r}_0)$ is assumed to be the two-dimensional free-space Green's function which can be represented by[13]

$$g(\underline{r}|\underline{r}_0) = (j/4)H_0(k_0|\underline{r}-\underline{r}_0|) \tag{4}$$

where $H_0(k_0|\underline{r}-\underline{r}_0|)$ is the zeroth-order Hankel function with first kind. If the argument of $H_0(k_0|\underline{r}-\underline{r}_0|)$ is much greater than unity, i.e., $k_0|\underline{r}-\underline{r}_0|>>1$, Eq.(4) can be simplified to

$$g(\underline{r}|\underline{r}_0) = \frac{j}{4}\sqrt{\frac{2}{\pi k_0|\underline{r}-\underline{r}_0|}}\exp[j(k_0|\underline{r}-\underline{r}_0|-\pi/4)] \tag{5}$$

As mentioned above, the incident wave is assumed to be a plane wave in the focal zone s and within the width of the beam strip (see Fig.1)

$$U_i(\underline{r}) = \begin{cases} A\exp(jk_0\underline{s}_0\cdot\underline{r}); & |x-x'|\leqslant L \\ 0 & ; \text{otherwise} \end{cases} \tag{6}$$

where A is a constant and $\underline{s}_0$ is a unit vector in the direction of the plane wave insonification.

Substituting Eq.(5) and Eq.(6) into Eq.(3), we obtain the expression of the scattered field measured on the point $(x',-l_0)$ when the center of transmitting group of the transducer elements is on the same point

$$U_s(x',-l_0;k_0) = \int_{-\infty}^{+\infty} F(x_0,y_0)A\exp(jk_0y_0)\frac{j}{4}\sqrt{\frac{2}{\pi k_0\sqrt{(x'-x_0)^2+(-l_0-y_0)^2}}} \cdot \exp[j(k_0\sqrt{(x'-x_0)^2+(-l_0-y_0)^2}-\pi/4)]dx_0\,dy_0 \tag{7}$$

where the notation k_0 in $U_s(x',-l_0;k_0)$ emphasizes the frequency dependence nature of the scattered field. Because the half-width of the incident beam L in Eq.(6) is very small, the integration in terms of the variable x_0 in Eq.(7) can be approximately looked as a constant. Therefore, from Eq.(7), one obtains

$$U_s(x',-l_0;k_0) = \int_{-\infty}^{+\infty} F(y_0)A'\exp(jk_0y_0)\frac{j}{4}\sqrt{\frac{2}{\pi k_0|-l_0-y_0|}} \cdot \exp[j(k_0|-l_0-y_0|-\pi/4)]dy_0 \tag{8}$$

where $A' = 2LA$ is a new constant and F(y) is the one-dimensional object function which is obtained by evaluating the two-dimensional object function $F(\underline{r})$ on the line $x = x'$ and is given below

$$F(y) = \begin{cases} k_0^2[n^2(x',y)-1]; & \text{if point } (x',y) \text{ is in the object} \\ 0 & ; \text{otherwise} \end{cases} \tag{9}$$

where $n(x',y) = c_0/c(x',y)$ is the distribution of the refractive index of the object on the line $x = x'$. For the convenience of the discussions in the following, two new functions which are related to the distribution of the refractive index of the object are defined

$$n_1(y) = F(y)/k_0^2 \tag{10}$$

$$n_e(y) = n_1(y)/\sqrt{l_0+y} \tag{11}$$

where $n_1(y)$ is another form of the object function and is assumed to be independent of the angular frequency ω; $n_e(y)$ is called equivalent object function. From Fig.1, one can see that l_0+y_0 is always greater than zero when the integral variable y_0 in Eq.(8) is confined to the focal zone s of the linear array probe. Therefore, from Eq.(8), we obtain

$$U_s(x',-l_0;k_0) = \frac{jA'k\delta\exp[j(k_0 l_0-\pi/4)]}{2\sqrt{2\pi k_0}}\tilde{n}_e(-2k_0) \tag{12}$$

where $\tilde{n}_e(k)$ represents the Fourier transform of the equivalent object function $n_e(y)$.

Taking the mechanical—electrical characteristics of the transducer into account, we have

$$P_s(x',-l_0;k_0) = P(k_0)\frac{jA'k\delta\exp[j(k_0 l_0-\pi/4)]}{2\sqrt{2\pi k_0}}\tilde{n}_e(-2k_0) \tag{13}$$

where $P_s(x',-l_0;k_0)$ represents the electrical signals produced by the returned rf echoes and $P(k)$ is the Fourier transform of the electrical—mechanical characteristic function. Eq.(13) can be written in another form

$$\tilde{n}_e(-2k_0) = \frac{2\sqrt{2\pi}\exp[-j(k_0 l_0+\pi/4)]}{k_0\sqrt{k_0}}\left[\frac{P_s(x',-l_0;k_0)}{P'(k_0)}\right] \tag{14}$$

where $P'(k_0) = A'P(k_0)$ and is calculated by

$$P'(k_0) = \frac{2\sqrt{2\pi l_0}\exp[-j(k_0 l_0+\pi/4)]}{k_0\sqrt{k_0}}P_{s\delta}(x',-l_0;k_0) \tag{15}$$

where $P_{s\delta}(x',-l_0;k_0)$ is the electrical signal produced by the echo returned from a point scatterer (for a point scatter, the object function $n_1(y)$ is of the form of Dirac—Delta function $\delta(y)$).

Frequency Extrapolation and Image Reconstruction

Because the incident wave and, therefore, the returned rf echoes are high center frequency band-pass acoustical signals, from Eq.(14), only the high-frequency component of the equivalent object function $n_e(y)$ can be obtained. To recover the low-frequency component of the equivalent object function from its high-frequency component, the Gerchberg-Papoulis (GP) frequency extrapolation technique is adopted and some available a priori knowledges are used in the frequency extrapolation.

The ordinary B-scanner can provide the outline information of the internal structures of the object, therefore, it is possible to determine the phases of the rf echo signals returned from these outlines. Fig.2 (a) and (b) are the waveforms of the rf echo signals returned from the water--agar and agar—water interfaces respectively. It is seen that their phases are different.

In order to use the phase information of the rf echo signals in the GP frequency extrapolation, it is required to know the relationship between the derivative of the equivalent object function and the measured the electrical signals produced by the returned rf echoes. Take the notations

Fig.2 (a) rf echo signals returned from the water–agar interface (b) from the agar–water interface

$n_e'(y)$ and $\tilde{n}_e'(k)$ as the derivative of the equivalent object function and its Fourier transform, from Eq.(14), we obtain

$$\tilde{n}_e'(-2k_0) = \frac{4\sqrt{2\pi}\exp[-j(k_0 l_0 + 3\pi/4)]}{\sqrt{k_0}} \left[\frac{P_s(x', -l_0; k_0)}{P'(k_0)}\right] \tag{16}$$

The procedures of the GP frequency extrapolation is described simply as follows:

(a) Calculate $\tilde{n}_e'^{(1)}(k)$, the high-frequency component of $n_e'(y)$, using Eq.(16) ($\tilde{n}_e'^{(1)}(k)$ is used to replace the high-frequency component of each order partial reconstruction of the equivalent object function in following iteration procedures).

(b) Find $n_e'^{(1)}(y)$, the first order partial reconstruction of the equivalent object function, by taking the IFFT of $\tilde{n}_e'^{(1)}(k)$.

(c) Determine the signs of $n_e'^{(1)}(y)$ on the outlines of the internal structures of the object in accordance with the phases of the rf echo signals returned from these outlines.

(d) Find $\tilde{n}_e'^{(2)}(k)$, the Fourier transform of the spatial modified $n_e'^{(1)}(y)$, by using the FFT.

(e) Substituting $\tilde{n}_e'^{(1)}(k)$ into the high-frequency portion of $\tilde{n}_e'^{(2)}(k)$ and then taking IFFT, we obtain $n_e'^{(2)}(y)$, the second order partial reconstruction of the equivalent object function.

(f) Calculate the average of $|n_e'^{(2)}(y) - n_e'^{(1)}(y)|$ and see if it is smaller than a preset small positive value. If the condition is true, go to step (g), otherwise, go back to step (c).

(g) Obtain the equivalent object function $n_e(y)$ by integrating $n_e'^{(N)}(y)$, the Nth order partial reconstruction of the equivalent object function (the integration constant is determined using the condition that $n_e(y) = 0$ if the point (x', y) is not in the object). By scanning the acoustical beam in a cross-section of the object, the equivalent object function $n_e(y)$ on different line $x = x'$ can be determined, and thus, tomographic image of the object can be reconstructed.

DESCRIPTION OF EXPERIMENTAL SYSTEM

Fig.3 is the block-diagram of the experimental system of the QRI

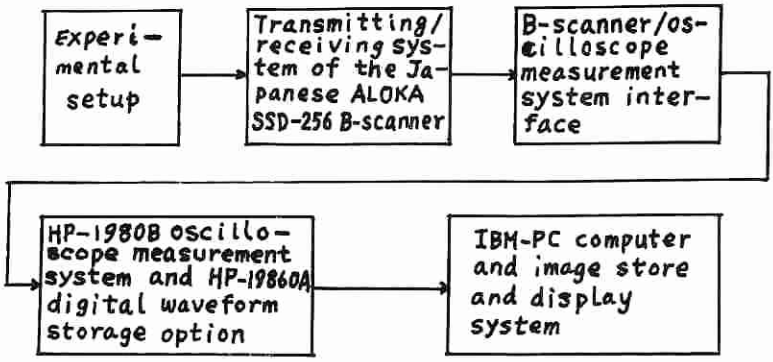

Fig.3 Experimental system for the QRI method

method. The experimental setup provides an acoustical environment for the datum acquisition. And the transmitting/receiving system of the Japanese ALOKA SSD-256 B-scanner[14] is used for the emission of the acoustical pulses and the reception of the rf echo signals returned from the testing objects. The signals received are transferred to HP-1980B oscilloscope measurement system[15] and sampled and quantized by HP-19860A digital waveform storage option[16] (to stabilize the datum acquisition, the B-scanner/oscilloscope measurement system interface which is developed by us is used). The digitized signals are then sent to IBM-PC computer through a standard IEEE-488 parallel interface for image reconstruction and the reconstructed images are transferred through a standard RS-232C serial interface to ARLUNYA TF-4000 temporal filter and image store, and, finally, displayed on the JVC high-resolution monitor.

EXPERIMENTAL RESULTS

Fig.4 shows cross-sectional figures of three agar phantoms prepared. The phantoms are even in the direction perpendicular to their transversal cross-sections. Fig.4(a) contains six small holes (one of them is of the diameter of 2 mm, and the others are of 3 mm) and is prepared from 4% agar aqueous solution. Fig.4(b) and (c) contain no hole and are prepared from 4% and 8% ager aqueous solution respectively. Fig.5 (a), (b) and (c) are the photographs of these phantoms and are corresponding to Fig.4 (a), (b) and (c) respectively.

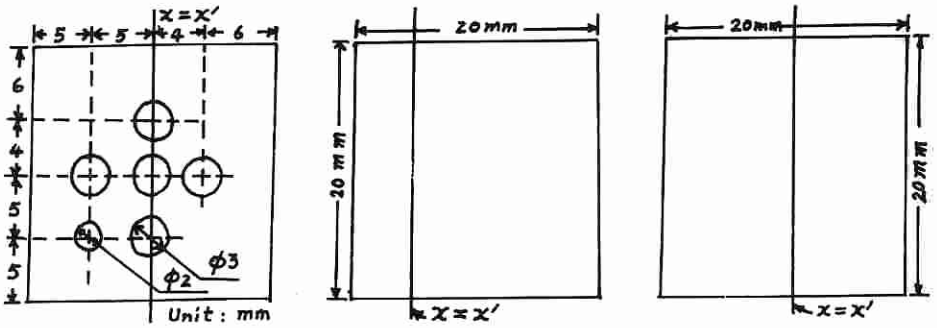

(a) (b) (c)

Fig.4 (a) Phantom with six holes (made of 4% agar aqueous solution), (b) and (c) Phantoms with no holes (made of 4% and 8% agar aqueous solution respectively)

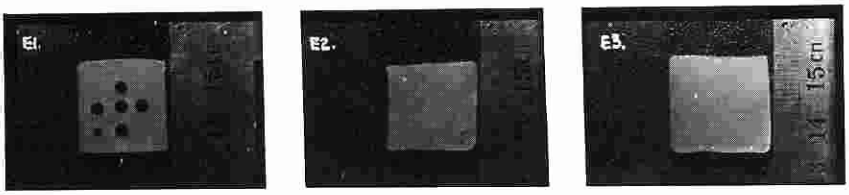

(a) (b) (c)

Fig.5 (a), (b) and (c) Photographs of the phantoms corresponding to Fig.4 (a), (b) and (c) respectively

To determine the electrical—mechanical characteristics of the transducer, a very thin silk with diameter of 0.04 λ (the center frequency of the acoustical pulses wave is about 3 MHz and the wave length λ in the biological soft-tissues is about 0.5 mm) is used as a point scatterer and is put on the focal point of the incident beam. Substituting the measured echo signals into Eq.(15), one can obtain the electrical—mechanical characteristics of the transducer.

Fig.6 (a), (b) and (c) are the images of the ordinary B-scanner and are corresponding to Fig.5 (a), (b) and (c) respectively. It is seen that these images can only provide the outline information of the internal structures of the testing objects. Fig.7 (a), (b) and (c) are the images reconstructed by the QRI method with the phantoms shown in Fig.5 (a), (b) and (c) respectively. Fig.8 (a), (b) and (c) are the comparisons of reconstructed values (real lines) of the images reconstructed by the QRI method and the real values (dashed lines) on the lines $x = x'$ shown in Fig.4 (a), (b) and (c), respectively. Because there is an experimentally determined constant A' in Eq.(13), the reconstructed values are only of relative meaning. Here, the reconstructed values averaged on the line $x = x'$ shown in Fig.4 (b) are taken as the reference for the comparisons. From Fig.6, Fig.7 and Fig.8, one can see that the images reconstructed by QRI method are more helpful in understanding the internal structures of the testing objects than the ordinary B-scan images, and to some extent, the images are quantitative.

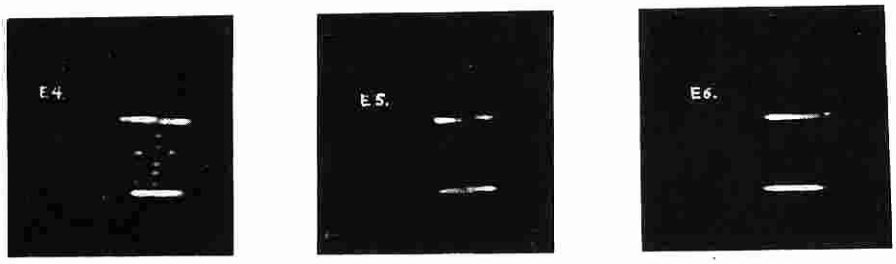

(a) (b) (c)

Fig.6 (a), (b) and (c) are the images obtained by the ordinary B-scanner and are corresponding to Fig.5 (a), (b) and (c) respectively

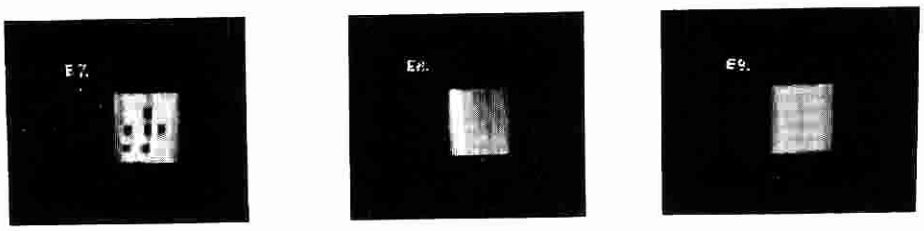

(a) (b) (c)

Fig.7 (a), (b) and (c) are the images reconstructed by the QRI method and are corresponding to Fig.5 (a), (b) and (c) respectively

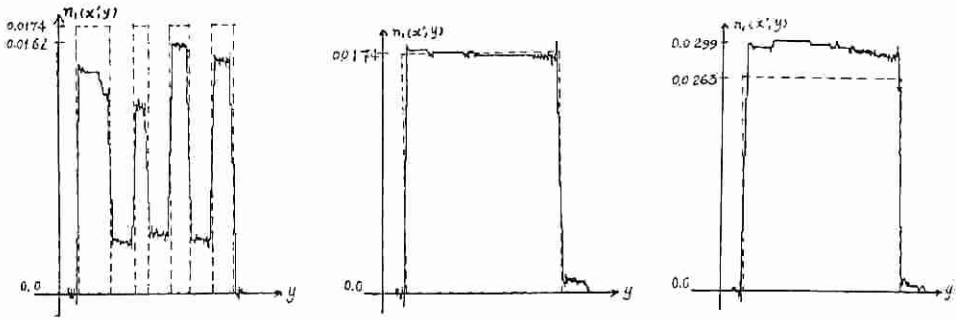

(a) (b) (c)

Fig.8 (a), (b) and (c) are the figures of the comparisons of the reconstructed values (real lines) of the images in Fig.7 and the real values (dashed lines) on the lines x = x' shown in Fig.4 (a), (b) and (c) respectively

SUMMARY

In this paper, a new quantitative reflection imaging method which employs the acoustical transmitting/receiving geometry of the ordinary B-scanner is developed. In addition to the theoretical analysis of this new imaging method, an experimental system is set up and images of the practical testing objects are reconstructed using the data obtained from this experimental system. The results show that the images reconstructed by the QRI method are more helpful in understanding the internal structures of the testing objects than the ordinary B-scan images and to some extent, the images are quantitative. Therefore, the QRI method will be useful in tissue characterization and will strengthen the abilities of the ordinary B-scanner in diagnosing the diseases.

Although the preliminary theoretical and experimental results obtained above, further researches (such as, considering the attenuation of the acoustical energy in the biological soft-tissues, taking into account the sound scattering caused by the inhomogeneities of the tissue density, improving the accuracy of the phase determination of the rf echo signals, using real time datum acquisition system and using practical biomedical soft-tissues as testing objects, etc.), must be continued if the QRI method is to be used in practical medical imaging.

REFERENCES

1. Jean-Pierre Ardouin and A. N. Venetsanopoulos, "Modelling and Restoration of Ultrasonic Phased-Array B-Scan Images", Ultrasonic Imaging, Vol.7, 1985, pp.321-344

2. M. Fatemi and A.C. Kak, "Ultrasonic B-Scan Imaging: Theory of Image Formation and a Technique for Restoration", Ultrasonic Imaging, Vol.2, 1980, pp.1-47

3. M.A. Fink and J.F. Cardoso, "Diffraction Effects in Pulse-Echo Measurement", IEEE Trans. Sonics & Ultrasonics, Vol.31, No.4, Jul.1984, pp.313-329

4. P.M. Gammell, "Improved Ultrasonic Detection Using the Analytic Signal Magnitude", Ultrasonics, Mar.1981, pp.73-76

5. G. Kossoff, "Progress in Pulse-Echo Techniques", Ultrasonics in Med., Exerpta Medica, No.309, 1974, pp.37-42

6. D.T. Kuan, A.A. Sawchuk, T.C. Strand and P. Chavel, "Adaptive Restoration of Images with Speckle", IEEE Trans. Acoustics, Speech and Signal Processing, Vol.35, No.3, Mar.1987, pp.373-383

7. M. O'Donnell, "Phase-Insensitive Pulse-Echo Imaging", Ultrasonic Imaging, Vol.4, 1982, pp.321-335

8. M. Ueda, "Computer Simulation of Artifacts in B-Mode Images", Proc. Ultrasonics Symposium, 1983, pp.718-721

9. R. Vaknine and W.J. Lorenz, "Lateral Filtering of Medical Ultrasonic B-Scans before Image Generation", Ultrasonic Imaging, Vol.6, 1984, pp.152-158

10. B. A. Roberts and A. C. Kak, "Reflection Mode Diffraction Tomography", Ultrasonic Imaging, Vol.7, 1985, pp.300-320

11. R.K. Mueller, M.Kaveh, and G. Wade, "Reconstructive Tomography and Applications to Ultrasonics" Proc. IEEE, Vol.67, No.4, 1979, pp.567-587

12. D. Nahamoo, S.X. Pan, and A.C. Kak, "Synthetic Aperture Diffraction Tomography and Its Interpolation-Free Computer Implementation", IEEE Trans. on Sonics and Ultrason., Vol.SU-31, No.4, Jul.1984, pp.218-229

13. P.M. Morse, H. Feshbach, "Methods of Theoretical Physics", McGraw-Hill, 1953

14. ALOKA Co. Ltd., Japan, "SSD-256 Training Manual".

15. HP Co. Ltd., America, "HP-1980A/B Oscilloscope Measurement System -- Operating Manual".

16. HP Co. Ltd., America, "HP-19860A Digital Waveform Storage Option -- Operating Manual".